

Successes and failures of simple statistical physics models for a network of real neurons

Leenoy Meshulam^{1,2}, Jeffrey L. Gauthier⁸, Carlos D. Brody^{3,6,7}, David W. Tank^{3,4,6}, and William Bialek^{4,5,9}

¹Center for Computational Neuroscience, and ²Department of Applied Mathematics, University of Washington, Seattle, Washington 98195

³Princeton Neuroscience Institute, ⁴Joseph Henry Laboratories of Physics,

⁵Lewis–Sigler Institute for Integrative Genomics, ⁶Department of Molecular Biology, and ⁷Howard Hughes Medical Institute, Princeton University, Princeton, NJ 08544

⁸Department of Biology, Swarthmore College, Swarthmore, Pennsylvania 19081 and

⁹Initiative for the Theoretical Sciences, The Graduate Center, City University of New York, 365 Fifth Ave., New York, NY 10016

(Dated: April 27, 2023)

Biological networks exhibit complex, coordinated patterns of activity. Can these patterns be captured precisely in simple models? Here we use measurements of simultaneous activity in 1000+ neurons in the mouse brain to test the validity of models grounded in statistical physics. When cells are dense samples from a small region, we find extremely detailed quantitative agreement between theory and experiment; sparse samples from larger regions lead to model failures. These results show we can aspire to more than qualitative agreement between simplifying theoretical ideas and the detailed behavior of a complex biological system.

Introduction. In statistical physics we routinely capture the behavior of complex systems, quantitatively, with models that are much simpler than the underlying microscopic mechanisms. Can we expect the same level of success in describing biological systems? Maximum entropy methods [1, 2] provide a direct path from data to simplified statistical physics models, and this has been used in systems ranging from protein families to flocks of birds [3–16]. In particular, these models accurately describe the activity distribution across populations of $N \sim 100$ cells in the dorsal hippocampus of mice [17]. But it is unclear whether these successes are significant: some authors claim these models describe only weak correlations [18, 19], while others worry that they are complex enough to make their success uninformative.

Recent progress in experimental methods creates new opportunities to test these theoretical ideas. Experiments now monitor 1000+ neurons in the hippocampus, which means we can choose groups of $N = 100$ cells in many different ways. We find that maximum entropy models which match pairwise correlations accurately predict higher order structure in the activity of spatially contiguous local subgroups, but not in distant subgroups where we draw the cells at random from a larger area. This aligns with evidence for spatial organization of neural activity in dorsal hippocampus [20–22]. Importantly, in the most successful examples all of the higher order statistical features of network activity that we test are predicted within experimental error. This sets a high standard for what we mean when we say that a model “works.”

Strategy. Experiments analyzed here monitor the activity of many neurons in the CA1 region of the mouse hippocampus [23, 24]. Briefly, mice have been genetically engineered to express GCaMP3, a calcium-sensitive fluorescent protein, and the resulting fluorescence is measured using a scanning two-photon microscope. The mouse runs on a floating ball while its head is fixed, and

rotation of ball is fed back to a visual stimulus to create the virtual experience of running along a 4 m track (Fig 1a). We focus on a data set with $N_{\text{total}} = 1485$ neurons (Fig 1b). Each experiment generates a $T \sim 40$ min time series of the fluorescence signal from each neuron (Fig 1c), with frames of duration $\Delta\tau = 1/30$ s. After denoising we binarize each neuron’s activity in each frame, based on whether it was active or silent, $\sigma_i \equiv \{0, 1\}$ [17].

Neurons in the hippocampus include “place cells” that are active only when the animal visits a particular location [25–27]. The network of place cells is thought to form a “cognitive map,” contributing to the animal’s navigation ability. In rodent CA1, 30–50% of neurons are place cells in any single experimental environment [17, 23, 27].

Assembling subgroups. To begin we choose a cell at random and draw a circle of radius $r = 0.07$ mm. This circle contains $N \sim 100$ cells, simulating previous generation of experiments with a more limited field of view [17], and we refer to these cells as a “local” subgroup of neurons. With the same cell at the center we draw larger circles— $r \sim 0.11, 0.14, 0.18, 0.22$ mm, increasing $2\times$ in area at each step—and then choose cells at random from these regions. For different groups to be comparable we want to keep the fraction of place cells fixed; this keeps the distribution of mean activities $\langle\sigma_i\rangle$ across the group roughly constant as well. Because the models we study are built by matching pairwise covariances,

$$C_{ij} = \langle(\sigma_i - \langle\sigma_i\rangle)(\sigma_j - \langle\sigma_j\rangle)\rangle, \quad (1)$$

we would also like to fix the distribution of these correlations. At radius r_k the distribution of matrix elements is $P_k(C)$; to expand $r_k \rightarrow r_{k+1}$ we swap cells in the smaller radius for those in the larger radius, and at every swap we minimize the Kullback–Leibler divergence between $P_k(C)$ and $P_{k+1}(C)$, until half of the cells have been swapped. This generates a nested collection of groups from progressively larger regions of the same brain area, matched in their basic statistical properties;

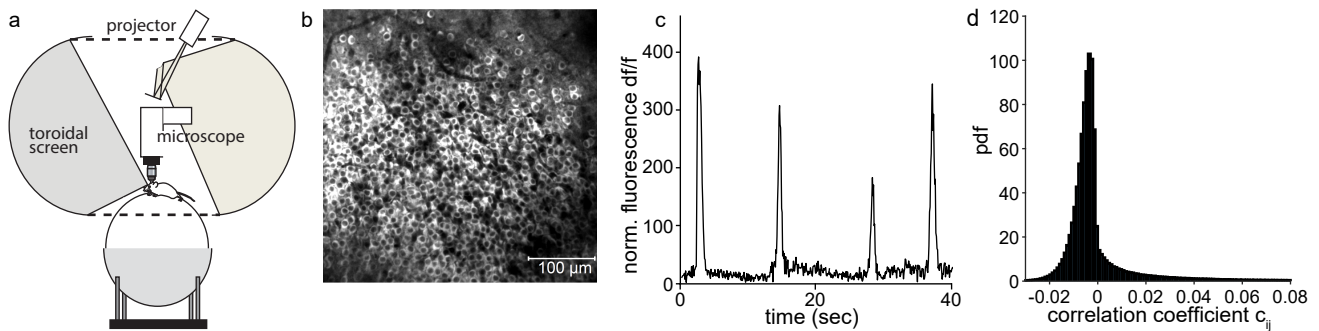


FIG. 1: **Experimental background.** (a) Schematic. A two-photon microscope is used to image large neuronal populations in a head-fixed mouse. Feedback from the animal running on the ball advances the virtual corridor projected on the toroidal screen. (b) Fluorescence image of 1485 neurons expressing calcium-sensitive fluorescent protein (averaged). (c) Sample trace of fluorescence from a single CA1 neuron, showing the high SNR. Raw data were motion corrected, normalized, and binarized [17]. (d) Probability distribution of correlation coefficients, $c_{ij} = C_{ij}/\sqrt{C_{ii}C_{jj}}$, across all pairs of neurons in (b).

Fig 2a shows an example of the smallest (“local”) and largest (“distant”) groups. These subgroups also simulate experiments that randomly sample a fraction of the cells in a region, down to $\sim 10\%$ at $r = 0.22$ mm.

Maximum entropy models for subgroups. In each of the subgroups we are faced with a population of $N = 100$ neurons, and in each small window of time ($\Delta\tau = 33$ ms) every cell either is active ($\sigma_i = 1$) or silent ($\sigma_i = 0$). The state of the entire network then is an N -bit binary vector $\{\sigma_i\} = \{\sigma_1, \sigma_2, \dots, \sigma_N\}$. A theory of the network should predict the probability that we find the system in any one of these states, $P(\{\sigma_i\})$, telling us how surprised we should be by any pattern of activity in the network.

The maximum entropy method constructs approximations to the distribution $P(\{\sigma_i\})$ that have as little structure as possible, or equivalently generate network states that are as random as possible, while matching some observed properties of the system [1, 2]. It is a theorem that the only way to make “as random as possible” mathematically precise is to maximize the entropy [28],

$$S = - \sum_{\{\sigma_i\}} P(\{\sigma_i\}) \log [P(\{\sigma_i\})]. \quad (2)$$

There is no unique choice for which properties of the system we should match. For a network of neurons, it makes sense to match the mean activity of every neuron,

$$\langle \sigma_j \rangle \equiv \sum_{\{\sigma_i\}} P(\{\sigma_i\}) \sigma_j = \langle \sigma_j \rangle_{\text{expt}}, \quad (3)$$

where $\langle \dots \rangle_{\text{expt}}$ is the average across the experiment. As a first step toward capturing the interactions among neurons in the network, we match the correlations between the activity in all pairs of cells jk ,

$$\langle \sigma_j \sigma_k \rangle \equiv \sum_{\{\sigma_i\}} P(\{\sigma_i\}) \sigma_j \sigma_k = C_{jk}^{\text{expt}} + \langle \sigma_j \rangle_{\text{expt}} \langle \sigma_k \rangle_{\text{expt}}. \quad (4)$$

The probability distribution that maximizes the entropy in Eq (2) while obeying the constraints in Eqs (3)

and (4) has the form

$$P(\{\sigma_i\}) = \frac{1}{Z} \exp[-E(\{\sigma_i\})] \quad (5)$$

$$E(\{\sigma_i\}) = - \sum_{i=1}^N h_i \sigma_i - \frac{1}{2} \sum_{i,j=1}^N J_{ij} \sigma_i \sigma_j. \quad (6)$$

$$Z = \sum_{\{\sigma_i\}} \exp[-E(\{\sigma_i\})]. \quad (7)$$

This is the statistical mechanics of Ising spins in magnetic fields h_i with couplings J_{ij} [29]. To complete the construction we have to find the $\{h_i, J_{ij}\}$. We use Monte Carlo to draw samples out of the distribution in Eqs (5–7), compute the expectation values $\langle \sigma_j \rangle$ and $\langle \sigma_j \sigma_k \rangle$, and adjust $\{h_i, J_{ij}\}$ until Eqs (3) and (4) are satisfied [17].

A crucial feature of the maximum entropy method is that once we have matched the measured mean activities and pairwise correlations, there are no free parameters. Thus we make *parameter-free* predictions for all the higher order statistical structure in the network. We have examples where these predictions have been successful [3, 11, 17], but this success is not guaranteed [30, 31].

Scope. For each dataset we have chosen ten different neurons as the center for the construction of subgroups described above, then built maximum entropy models for local and distant subgroups of $N = 100$ cells. We focus on one typical example; populations at intermediate radii interpolate between the extremes described here, and results are consistent across all examples from three different mice. We look at six different predictions, contrasting the levels of success in local and distant subgroups.

Simultaneous activity. The maximum entropy model aims to capture the *collective* nature of population activity. A first test is to ask for the probability that K out of the N neurons are active in the same small window of time, $P(K)$. Figure 2e shows this distribution for the local subgroup, and Fig 2f shows the same distribution for the distant one. The local subgroup predictions stay within experimental error bars throughout the entire

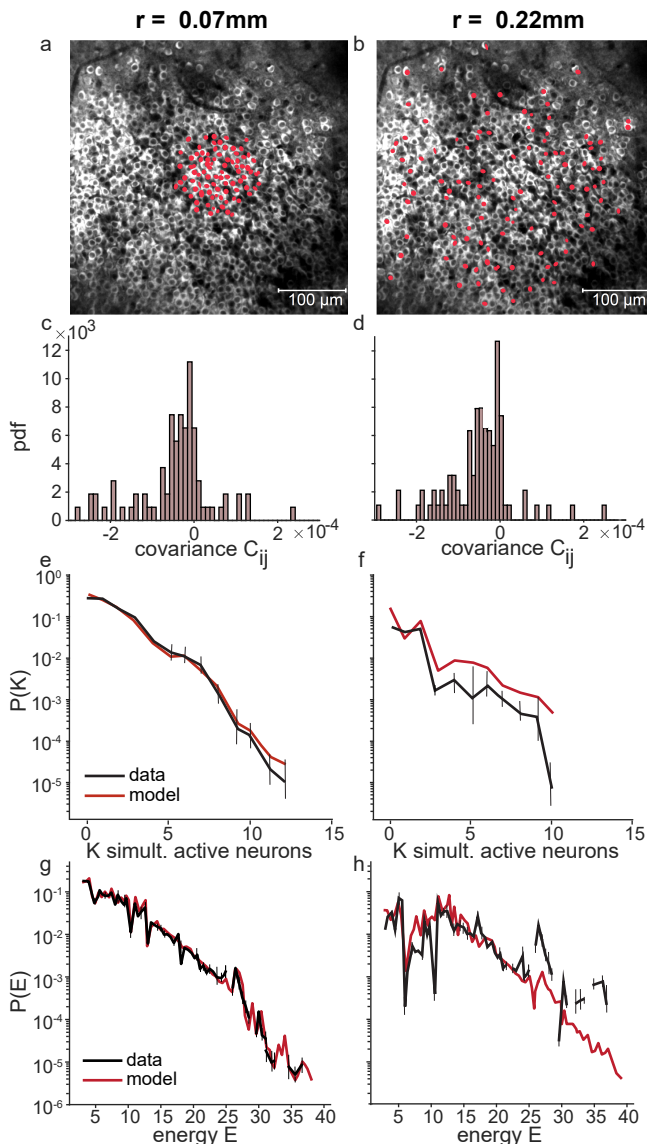


FIG. 2: **Theory and experiment for “local” (left: a, c, e, g) and “distant” (right: b, d, f, h) subgroups.** (a, b) Fluorescence image of the entire field of view, as in Fig 1b. Red marks are the cells included in example local (a) and distant (b) subgroups. (c, d) Probability distributions of covariances C_{ij} for the subgroups in (a) and (b), respectively. (e, f) The probability that K out of the $N = 100$ neurons in the subgroup population are active simultaneously. (g, h) The distribution of effective energies, $P(E)$, across all network states. In (e–h), predictions in red, mean and standard deviations over random halves of the data in black.

range, even down to probabilities $10^{-4} - 10^{-5}$ at $K > 10$. In contrast, the distant subgroup predictions are out of measurement error bounds for all $K > 3$.

Density of states. The fundamental object of our models is the effective energy $E(\{\sigma_i\})$ assigned to every network state. We can look at the distribution $P(E)$ across the experimentally observed states, as well as the distribution predicted from the theory itself. Predictions are

in excellent quantitative agreement with experiment for the local subgroup (Fig 2g), including details that one might be tempted to dismiss as noise but in fact are significant. Agreement extends to $E > 30$, corresponding to individual network states with relative probabilities of $\sim 10^{-13}$. In contrast, predictions in the distant subgroup fail already at $E \sim 7$ (Fig 2h).

Triplet correlations. We have constructed models that match correlations between pairs of neurons, so a natural test of the theory is to predict correlations among triplets,

$$C_{ijk} \equiv \langle (\sigma_i - \langle \sigma_i \rangle) (\sigma_j - \langle \sigma_j \rangle) (\sigma_k - \langle \sigma_k \rangle) \rangle. \quad (8)$$

For $N = 100$ cells there are $\sim 1.6 \times 10^5$ distinct triplets. In Figs 3a and b we group these into bins, showing the mean and standard deviation in each bin, plotting measured vs predicted values. For the local subgroup, predictions are within experimental error across the full dynamic range of the data (Fig 3a). For the distant subgroup, in contrast, there is a dramatic mismatch between theory and experiment (Fig 3b).

Individual triplets. As a more stringent test we scrutinize each of the $\sim 1.6 \times 10^5$ triplets individually. Concretely, we compute the root-mean-square (rms) difference between each predicted and measured correlation (inside small bins) as well as the rms error in our measurements. For the local subgroup, prediction errors track measurement errors (Fig 3c); it is almost impossible to do better without over-fitting. Errors in the distant subgroup are much larger, including for the smallest and most frequent values of C_{ijk} (Fig 3d).

Effective fields. As usual with Ising models we can define an effective field h_i^{eff} ,

$$h_i^{\text{eff}} = E(\sigma_1, \dots, \sigma_i = 0, \dots, \sigma_N) - E(\sigma_1, \dots, \sigma_i = 1, \dots, \sigma_N) \quad (9)$$

$$= h_i + \sum_{j \neq i} J_{ij} \sigma_j, \quad (10)$$

which predicts how the network state influences probability that a single neuron is active,

$$q \equiv P(\sigma_i = 1 | h_i^{\text{eff}}) = \frac{1}{1 + \exp(-h_i^{\text{eff}})}. \quad (11)$$

In Figs 3e and f we test these predictions: we obtain an effective field value for each neuron at every moment in time given the state of the rest of the population, and then pool all of these values together. Each panel depicts the probability of a neuron to be active against the effective field of the same neuron, on top of the prediction from Eq (11). Again the agreement between theory and observations is very good for the local subgroup (Fig 3e), even for very large effective fields, while prediction quality drops in the distant subgroup (Fig 3f).

Inferring the field. Does a neuron being active (silent) predict a high (low) value of the effective field? This is related to Eq (11) via Bayes rule:

$$P(h_i^{\text{eff}} | \sigma_i) = \frac{P(\sigma_i | h_i^{\text{eff}}) P(h_i^{\text{eff}})}{P(\sigma_i)}. \quad (12)$$

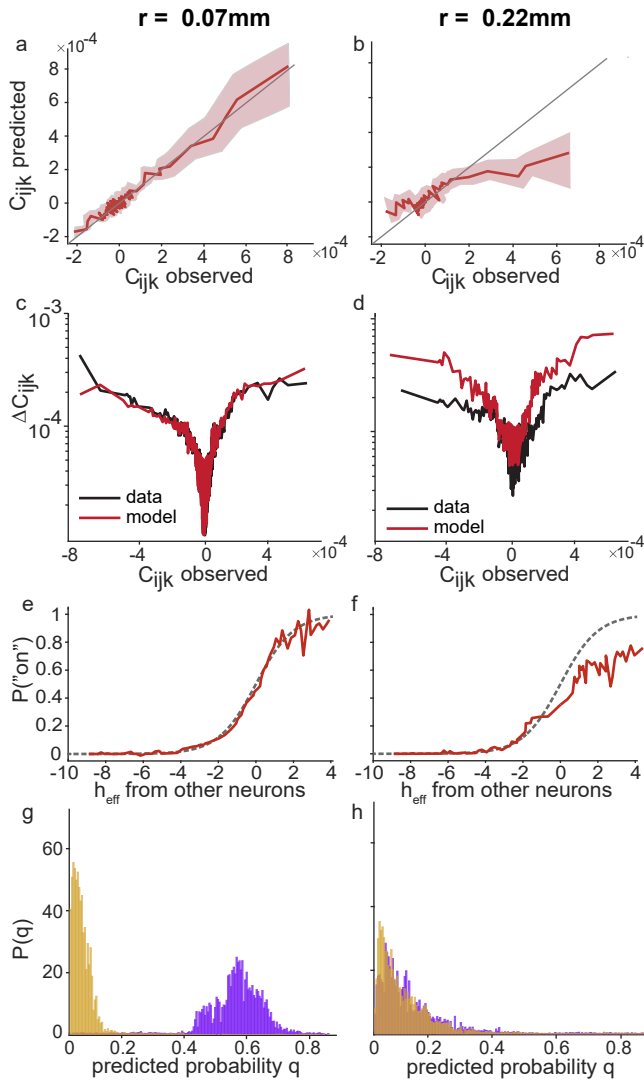


FIG. 3: **Triples and effective fields in local (left: a, c, e, g) and distant (right: b, d, f, h) subgroups.** (a, b) Comparison of the maximum entropy model predictions for triplet correlations, C_{ijk} , with experiment. All $N^3/3 \sim 10^5$ values are binned, adaptively, along the x-axis, showing mean (red line) and standard deviation (shading). (c, d) Root-mean-square errors of individual predictions (red) and measurements (black). (e, f) Probability of neuron to be active $\sigma_i = 1$ vs effective field h_i^{eff} . Data in red, parameter-free prediction from Eq (10) shown as dashed black line. (g, h) Conditional probability of effective field, expressed as q from Eq (11), given the state of the neuron, $P(h_i^{\text{eff}}|\sigma_i)$, with $\sigma_i = 1$ in purple and $\sigma_i = 0$ in yellow.

There is no “correct” distribution of h_{eff} , but it would be attractive if neurons being active predicted that the

whole network is in a state that favors this activity [large q in Eq (11)]; conversely silent neurons should predict small q . Figures 3g and h show the distributions $P(q|\sigma)$, assembled by sampling all moments in time when a neuron was active or silent. A clear separation between the two distributions indicates that our model really does distinguish network states that drive activity or silence of individual cells. This works for the local subgroup (Fig 3g) but not for the distant subgroup (Fig 3h).

Discussion. It has never been clear whether relatively simple statistical physics models for networks of neurons should be taken seriously as quantitative theories. The class of models we have considered is based on the idea that all structure in neural activity is encoded in the matrix of pairwise correlations; all subsequent predictions (as in Figs 2 and 3) are parameter-free. We draw three main conclusions. First, parameter-free predictions of simple theories can agree with real biological data in surprising quantitative detail: for local subgroups, all predictions we test agree with experiment within measurement errors. Second, this is not guaranteed: we can choose different groups of $N = 100$ neurons from the same area of the brain, with similar patterns of mean activity and pairwise correlations in response to the same behaviors, and predictions of the simple model fail. These results are reproduced in thirty different local/distant subgroup pairs across three different mice.

A corollary is that we need to be careful in saying that we have agreement or disagreement between theory and experiment. Looking only at distant subgroups one might be tempted to say that we capture trends in the data, and that the lack of quantitative agreement is the result of over-simplification. But this is not the case, since we achieve detailed quantitative agreement using the same theory to describe a different group of cells in the same area under the same conditions. This leads to a third conclusion, that success or failure of our predictions reflects properties of the underlying network. Success is found when we describe a densely sampled collection of cells from a contiguous region, suggesting that effective interactions are local; drawing a tight circle around $N = 100$ cells we come closer to capturing a complete network.

Work supported in part by the National Science Foundation through the Center for the Physics of Biological Function (PHY-1734030); by the Simons Collaboration on the Global Brain; by the Howard Hughes Medical Institute; and by the Swartz Foundation. This paper is dedicated to the memory of Cristina Domnisoru, a luminary who inspired so many; a continuing source of brilliance, creativity, and wonder. Cristina burned selflessly and incisively to better the world, and leaves a lasting echo in her wake.

[1] ET Jaynes. Information theory and statistical mechanics. *Phys. Rev.*, 106(4):620, 1957.

[2] ET Jaynes. On the rationale of maximum-entropy methods. *Proc. IEEE*, 70(9):939–952, 1982.

- [3] E Schneidman, MJ Berry II, R Segev, and W Bialek. Weak pairwise correlations imply strongly correlated network states in a neural population. *Nature*, 440(7087):1007–1012, 2006.
- [4] G Tkačik, E Schneidman, MJ Berry II, and W Bialek. Ising models for networks of real neurons. *arXiv preprint q-bio/0611072*, 2006.
- [5] G Tkačik, E Schneidman, MJ Berry II, and W Bialek. Spin glass models for a network of real neurons. *arXiv preprint arXiv:0912.5409*, 2009.
- [6] IE Ohiorhenuan, F Mechler, KP Purpura, AM Schmid, Q Hu, and JD Victor. Sparse coding and high-order correlations in fine-scale cortical networks. *Nature*, 466(7306):617–621, 2010.
- [7] T Mora, AM Walczak, W Bialek, and CG Callan, Jr. Maximum entropy models for antibody diversity. *Proc. Natl. Acad. Sci. (USA)*, 107(12):5405–5410, 2010.
- [8] DS Marks, LJ Colwell, R Sheridan, TA Hopf, A Pagnani, R Zecchina, and C Sander. Protein 3d structure computed from evolutionary sequence variation. *PLoS One*, 6(12):e28766, 2011.
- [9] A Lapedes, B Giraud, and C Jarzynski. Using sequence alignments to predict protein structure and stability with high accuracy. *arXiv preprint arXiv:1207.2484*, 2012.
- [10] W Bialek, A Cavagna, I Giardina, T Mora, E Silvestri, M Viale, and AM Walczak. Statistical mechanics for natural flocks of birds. *Proc. Natl. Acad. Sci. (USA)*, 109(13):4786–4791, 2012.
- [11] E Granot-Atedgi, G Tkačik, R Segev, and E Schneidman. Stimulus-dependent maximum entropy models of neural population codes. *PLoS Comput. Biol.*, 9(3):e1002922, 2013.
- [12] W Bialek, A Cavagna, I Giardina, T Mora, O Pohl, E Silvestri, M Viale, and AM Walczak. Social interactions dominate speed control in poisoning natural flocks near criticality. *Proc. Natl. Acad. Sci. (USA)*, 111(20):7212–7217, 2014.
- [13] L Asti, G Uguzzoni, P Marcatili, and A Pagnani. Maximum-entropy models of sequenced immune repertoires predict antigen-antibody affinity. *PLoS Comput. Biol.*, 12(4):e1004870, 2016.
- [14] A-F Bitbol, RS Dwyer, LJ Colwell, and NS Wingreen. Inferring interaction partners from protein sequences. *Proc. Natl. Acad. Sci. (USA)*, 113(43):12180–12185, 2016.
- [15] G Tavoni, U Ferrari, FP Battaglia, S Cocco, and R Monasson. Functional coupling networks inferred from prefrontal cortex activity show experience-related effective plasticity. *Netw. Neurosci.*, 1(3):275–301, 2017.
- [16] WP Russ, M Figliuzzi, C Stocker, P Barrat-Charlaix, M Socolich, P Kast, D Hilvert, R Monasson, S Cocco, M Weigt, and R Ranganathan. An evolution-based model for designing chorismate mutase enzymes. *Science*, 369(6502):440–445, 2020.
- [17] L Meshulam, JL Gauthier, CD Brody, DW Tank, and W Bialek. Collective behavior of place and non-place neurons in the hippocampal network. *Neuron*, 96(5):1178–1191, 2017.
- [18] Y Roudi, S Nirenberg, and PE Latham. Pairwise maximum entropy models for studying large biological systems: when they can work and when they can't. *PLoS Comput. Biol.*, 5(5):e1000380, 2009.
- [19] JH Macke, I Murray, and PE Latham. How biased are maximum entropy models? In *NeurIPS*, pages 2034–2042, 2012.
- [20] SI Wiener, CA Paul, and H Eichenbaum. Spatial and behavioral correlates of hippocampal neuronal activity. *J. Neurosci.*, 9(8):2737–2763, 1989.
- [21] RE Hampson, JD Simeral, and SA Deadwyler. Distribution of spatial and nonspatial information in dorsal hippocampus. *Nature*, 402(6762):610–614, 1999.
- [22] JP Rickgauer, K Deisseroth, and DW Tank. Simultaneous cellular-resolution optical perturbation and imaging of place cell firing fields. *Nat. Neurosci.*, 17(12):1816–1824, 2014.
- [23] JL Gauthier and DW Tank. A dedicated population for reward coding in the hippocampus. *Neuron*, 99(1):179–193, 2018.
- [24] JL Gauthier, SA Koay, EH Nieh, DW Tank, JW Pillow, and AS Charles. Detecting and correcting false transients in calcium imaging. *bioRxiv*, page 473470, 2018.
- [25] J O'Keefe and L Nadel. *The Hippocampus as a Cognitive Map*. Oxford university press, 1978.
- [26] J O'Keefe. A review of the hippocampal place cells. *Prog. Neurobiol.*, 13(4):419–439, 1979.
- [27] DA Dombeck, CD Harvey, L Tian, LL Looger, and DW Tank. Functional imaging of hippocampal place cells at cellular resolution during virtual navigation. *Nat. Neurosci.*, 13(11):1433–1440, 2010.
- [28] CE Shannon. A mathematical theory of communication. *The Bell Syst. Tech. J.*, 27(3):379–423, 1948.
- [29] M Mézard, G Parisi, MA Virasoro, and DJ Thouless. Spin glass theory and beyond. *Phys. Today*, 41(12):109, 1988.
- [30] E Ganmor, R Segev, and E Schneidman. Sparse low-order interaction network underlies a highly correlated and learnable neural population code. *Proc. Natl. Acad. Sci. (USA)*, 108(23):9679–9684, 2011.
- [31] G Tkačik, O Marre, D Amodei, E Schneidman, W Bialek, and MJ Berry. Searching for collective behavior in a large network of sensory neurons. *PLoS Comput. Biol.*, 10(1):e1003408, 2014.